PHYSICS OF FLUIDS **28**, 042105 (2016)

The necking time of gas bubbles in liquids of arbitrary viscosity

R. Bolaños-Jiménez,[1,a)] A. Sevilla,[2,b)] and C. Martínez-Bazán[1,c)]
[1]*Área de Mecánica de Fluidos, Departamento de Ingeniería Mecánica y Minera, Universidad de Jaén, Campus de las Lagunillas, 23071 Jaén, Spain*
[2]*Área de Mecánica de Fluidos, Departamento de Ingeniería Térmica y de Fluidos, Universidad Carlos III de Madrid, 28911 Leganés, Spain*

(Received 10 January 2016; accepted 17 March 2016; published online 6 April 2016)

We report an experimental and theoretical study of the collapse time of a gas bubble injected into an otherwise stagnant liquid under quasi-static conditions and for a wide range of liquid viscosities. The experiments were performed by injecting a constant flow rate of air through a needle with inner radius a into several water/glycerine mixtures, providing a viscosity range of 20 cP $\lesssim \mu \lesssim$ 1500 cP. By analyzing the temporal evolution of the neck radius, $R_0(t)$, the collapse time has been extracted for three different stages during the collapse process, namely, $R_i/a = 0.6$, 0.4, and 0.2, being $R_i = R_0(t = 0)$ the initial neck radius. The collapse time is shown to monotonically increase with both R_i/a and with the Ohnesorge number, $Oh = \mu/\sqrt{\rho\sigma R_i}$, where ρ and σ represent the liquid density and the surface tension coefficient, respectively. The theoretical approach is based on the cylindrical Rayleigh-Plesset equation for the radial liquid flow around the neck, which is the appropriate leading-order representation of the collapse dynamics, thanks to the slenderness condition $R_0(t)\, r_1(t) \ll 1$, where $r_1(t)$ is half the axial curvature of the interface evaluated at the neck. The Rayleigh-Plesset equation can be integrated numerically to obtain the collapse time, τ_{col}, which is made dimensionless using the capillary time, $t_\sigma = \sqrt{\rho R_i^3/\sigma}$. We present a novel scaling law for τ_{col} as a function of R_i/a and Oh that closely follows the experimental data for the entire range of both parameters, and provide analytical expressions in the inviscid and Stokes regimes, i.e., $\tau_{col}(Oh \to 0) \to \sqrt{2 \ln C}$ and $\tau_{col}(Oh \to \infty) \to 2Oh$, respectively, where C is a constant of order unity that increases with R_i/a. © *2016 AIP Publishing LLC.* [http://dx.doi.org/10.1063/1.4944973]

I. INTRODUCTION

Bubble generation in viscous liquids constitutes a matter of increasing interest in many applications related with magma, polymer melts, or molten metals and glasses, among many others (see Ref. 1 and references therein). In particular, the formation of a bubble that grows quasi-statically from a submerged injector inside a stagnant liquid has been the most studied configuration, due to its simplicity and importance in many engineering applications. Nevertheless, most of the studies about bubble formation inside quiescent liquids have been devoted to the case of inviscid liquids (see Refs. 2–8, among others). The bubbles generated under quasi-static conditions have almost the same size, determined by a quasi-static balance between surface tension and buoyancy forces, leading to the so-called Fritz volume, $V_F = 2\pi\sigma a/(\rho g)$, where σ is the surface tension coefficient, a is the inner injector radius, and ρ is the liquid density. This quasi-static regime prevails when the gas flow rate is smaller than a critical value of the order of $Q_c \simeq \pi(16/3g^2)^{1/6}(\sigma\, a/\rho)^{5/6}$ for inviscid

a)Electronic mail: rbolanos@ujaen.es
b)Electronic mail: asevilla@ing.uc3m.es
c)Electronic mail: cmbazan@ujaen.es

liquids[9] and $Q_c \simeq \rho g V_F^{4/3}/\mu$ for viscous liquids.[10] Under these conditions, the bubble formation can be described as a two-stage phenomenon.[9] On the one hand, after the detachment of the previous bubble, a quasi-static *expansion stage* begins, where the gas stem that remains attached to the injector tip grows axially and radially until the forming bubble is large enough for the buoyancy force to overtake the surface tension force. On the other hand, the expansion stage is followed by a dynamic *collapse stage*, where a neck appears at the interface in the vicinity of the nozzle exit, the bubble shape becomes unstable, and the neck accelerates radially inwards leading to its pinch-off and the consequent detachment of the forming bubble.

In the present work, we focus on the duration of the collapse stage and its dependence on the liquid viscosity. Previous works on the subject have been devoted to analyze the neck shrinking phenomenon, but only during the last instants, previous to the pinch-off of the bubble, which has been traditionally described by a power law $(R_0/a) \sim (\tau_{col} - \tau)^{\alpha}$, where R_0 is the radius of the neck and $(\tau_{col} - \tau)$ indicates the dimensionless time remaining to pinch-off. In the inviscid limit, it is now well established that $\alpha \gtrsim 1/2$, its exact value depending on the initial conditions and actually varying during the collapse process.[4,6,8,11–16] The effect of liquid viscosity on the global collapse time of a bubble has been comparatively less studied. In the Stokes limit of negligible liquid inertia, the balance between surface tension and viscous forces in the surrounding liquid gives a minimum radius that decreases linearly with time[6,11,17] and correspondingly $\alpha = 1$. For intermediate values of liquid viscosity, referred to as the *transition regime* by Burton *et al.*[11] and Thoroddsen *et al.*,[6] α is observed to increase from the inviscid to the Stokes value, $1/2 \lesssim \alpha \leq 1$, as the liquid viscosity increases. This transition range has also been investigated by Bolaños-Jiménez *et al.*,[17] where it was revealed that the local Reynolds number, $\mathrm{Re}_l = \rho R_0 \dot{R}_0/\mu$, where the dot indicates time derivative, becomes $O(1)$ during the collapse process. Correspondingly, the instantaneous exponent $\alpha(\tau)$ increases during pinch-off from $\alpha \gtrsim 0.58$ when $\mathrm{Re}_l \gtrsim O(1)$ to $\alpha \simeq 1$ when $\mathrm{Re}_l \ll 1$. In Ref. 17, it is also shown that an alternative description of the last instants prior to pinch-off reproduces the experimental results in the entire range of liquid viscosities, including the smooth transition from the inviscid to the viscous-dominated pinch-off that takes place within the previously mentioned transition regime of intermediate liquid viscosities.

All the aforementioned works on the bubble collapse stage are devoted to the description of the dynamics only during the last instants prior to break-up. There are also many previous studies focused on the effect of the liquid viscosity on general characteristics of the gas bubble, such as its size, shape, rise behavior, and coalescence.[18–24] However, the main goal of the present work is to experimentally characterize in detail the duration of the collapse stage of a bubble generated quasi-statically as a function of the liquid viscosity, starting from neck radii of the order of the injector radius, as well as to provide a simple scaling law for the global necking time. The paper is structured as follows. Section II is devoted to describe the experimental facility, the experimental conditions, and the control parameters, as well as the techniques used to analyze the images recorded in the experiments. In Section III, the problem is analyzed by means of theory. In particular, the cylindrical Rayleigh-Plesset equation is used to describe the radial flow in the slender neck region and linearized to obtain a scaling law for the collapse time as a function of the Ohnesorge number. Finally, Section IV summarizes the main conclusions.

II. EXPERIMENTAL MEASUREMENTS

To investigate the influence of liquid viscosity on the bubble collapse time, several sets of experiments were performed using the facility described in Bolaños-Jiménez *et al.*.[17] It consists of an injector of inner radius a located at the bottom of a reservoir made of Plexiglas, through which a constant air flow rate, Q, was injected (see Figs. 1(a) and 1(b)). The gas feeding system was designed such that the influence of Q is negligible, and therefore, the bubbling process takes place under quasi-static conditions. The bubbles generated under these conditions have practically the same size regardless of Q, determined by a balance between surface tension and buoyancy forces, leading to the so-called *Fritz Volume*, $V_F = 2\pi\sigma a/(\rho g)$. In this regime, the inertial and viscous forces in the liquid are negligible during the bubble expansion stage but become important

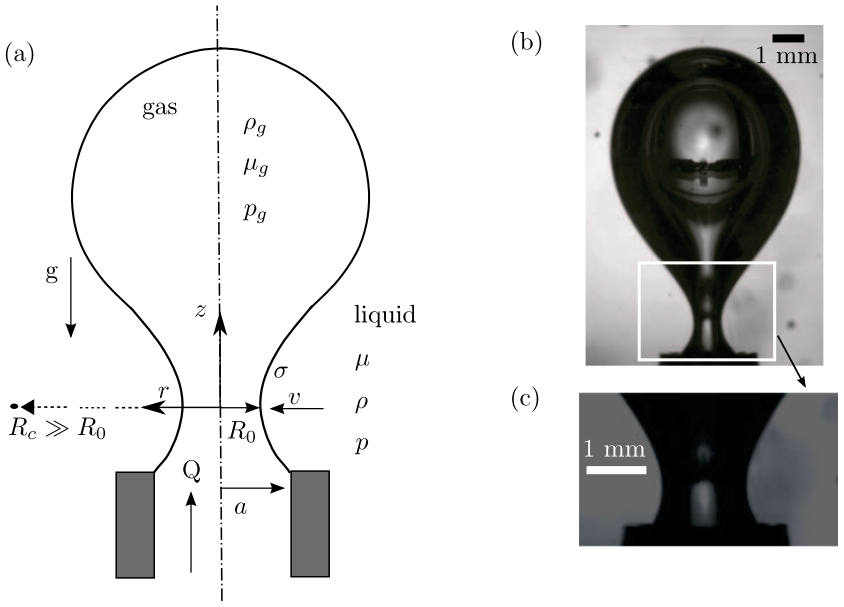

FIG. 1. (a) Sketch of the flow configuration with the physical parameters. R_c is a point placed sufficiently far away from the neck. (b) Image extracted from a high-speed movie (10 000 fps), showing the entire collapsing bubble in a water-glycerine mixture (experiment G7 in Table I). (c) Image corresponding to the same experimental conditions shown in (b) but taken from a 50 000 fps movie recorded at the length scale of the needle radius.

during the collapse stage studied herein. To confirm that quasi-static conditions were accomplished, the final volume of the bubble, V_B, was extracted from the experiments, obtaining $V_B \simeq V_F$ in all cases. The liquid viscosity μ was varied by using six different water/glycerine mixtures, achieving a range of 20 cP $\lesssim \mu \lesssim$ 1500 cP. Moreover, two different needles with inner radii of 1.025 and 2.55 mm were employed, as reported in Table I. The mixtures were carefully prepared by measuring the glycerine mass fraction, x, with an accuracy of ±0.02 g in the measurements of the water and glycerine masses. The homogeneity of the mixtures was ensured by a slow stirring process that avoided the entrance of ambient air. The density and the viscosity were first measured at room temperature before performing the experiments and compared with the values obtained from interpolation of high-precision Dow Corning tables as a function of both the mass fraction, x, and temperature, T, obtaining a good agreement. This validated the use of the Dow Corning tables and

TABLE I. Summary of the experiments performed using glycerin-water mixtures, together with the values of the dimensional parameters and the Ohnesorge number defined with the needle radius, $Oh_a = \mu/\sqrt{\rho\,\sigma\,a}$. Here, x indicates the glycerin mass fraction. The relative errors in density and surface tension are smaller than 1% in all cases.

Expt.	a (mm)	x (%)	T (°C)	ρ (kg/m^3)	σ (N/m)	μ (cP)	Oh_a
G1	1.025	70	18.6	1182	0.0669	24.3 ± 0.6	0.085 ± 0.004
G2	1.025	83	20.2	1216	0.0652	88.1 ± 2.8	0.309 ± 0.017
G3	1.025	91	19.5	1235	0.0642	229.4 ± 10.2	0.80 ± 0.05
G4	1.025	95	16.6	1251	0.0635	686.9 ± 31.6	2.41 ± 0.17
G5	1.025	97	17.3	1256	0.0632	965.6 ± 45.3	3.4 ± 0.2
G6	1.025	99	17.8	1261	0.0629	1411.9 ± 66.2	4.9 ± 0.3
G7	2.550	70	18.8	1182	0.0669	24.1 ± 0.6	0.053 ± 0.002
G8	2.550	83	21.4	1216	0.0651	81.8 ± 2.5	0.182 ± 0.007
G9	2.550	91	20.2	1235	0.0642	217.4 ± 9.6	0.48 ± 0.03
G10	2.550	95	18.2	1250	0.0635	597.7 ± 26.8	1.33 ± 0.07
G11	2.550	97	20.7	1254	0.0631	714.7 ± 31.6	1.59 ± 0.09
G12	2.550	99	17.4	1261	0.0629	1466.8 ± 66.2	3.26 ± 0.19

confirmed the homogeneity of the mixtures. Thus, the values of the properties reported in Table I are the results given by the Dow Corning tables using the temperature registered during the experiment, which was precisely monitored and controlled with a temperature probe (accuracy of ±0.5 °C) placed inside the liquid pool. The accuracy of the temperature and mass measurements resulted in some uncertainty in the corresponding viscosity and, consequently, in the Ohnesorge number based on the needle radius $Oh_a = \mu/\sqrt{\rho\,\sigma\,a}$, as reported in Table I, with a maximum relative error of ≃5% in the viscosity and ≃7% in Oh_a, which also included the accuracy in the measurements of the injector radius (±0.05 mm). Since the present work focuses on the global collapse process, high-speed movies at the scale of the needle radius were recorded at 50 000 fps (Fig. 1(c)) with spatial resolutions between 16 and 33 μm/pixel.

The physical parameters governing our experiment are the inner radius of the needle a, the surface tension coefficient σ, the gravitational acceleration g, the air flow rate Q, the densities of both the liquid, ρ, and the gas, ρ_g, and the liquid and gas viscosities, μ and μ_g, respectively. As shown in Bolaños-Jiménez *et al.*,[17] the influence of the gas density, $\rho_g \ll \rho$, and viscosity, $\mu_g \ll \mu$, can be neglected except in the last few microseconds prior to pinch-off,[25] and the pressure can be considered spatially uniform inside the bubble. Therefore, the collapsing process is controlled by only two dimensionless parameters, namely, the Bond number, $Bo = \rho\, g\, a^2/\sigma$, and the Reynolds number, $\mathrm{Re} = \rho\, v_\sigma\, R_i/\mu = 1/Oh$, where $v_\sigma = \sqrt{\sigma/(\rho R_i)}$ is the capillary velocity, R_i the initial radius of the neck, and $Oh = \mu/\sqrt{\rho\,\sigma\,R_i}$ the Ohnesorge number based on the initial neck radius. Notice that, for convenience, the initial neck radius, $R_i = R_0(t = 0)$, has been used in the present work as characteristic length scale, instead of the nozzle radius, a, used in Ref. 17. Thus, the Ohnesorge number defined with the nozzle radius is $Oh_a = Oh\sqrt{R_i/a}$. The value of Oh_a for the different liquid mixtures used in the present study can be found in Table I.

The experimental results were obtained from the high-speed movies using standard edge-finding routines. In particular, the temporal evolution of the neck radius, $R_0(t)$, was analyzed to investigate the influence of the liquid viscosity on the collapse time, as can be observed in Figs. 2(a) and 2(b). The collapse time t_{col}, defined such that $R_0(t_{col}) = 0$, was obtained for each experimental run by extrapolating the last ten values of R_0 prior to pinch-off. The resulting value had an uncertainty of one frame (0.02 ms) in all the cases except in the most viscous ones (G5, G6, G12), where the uncertainty increases to 2 or 3 frames due to the formation of a thin air thread before the bubble pinch-off. The final value of t_{col} for each experiment was determined by averaging the results of

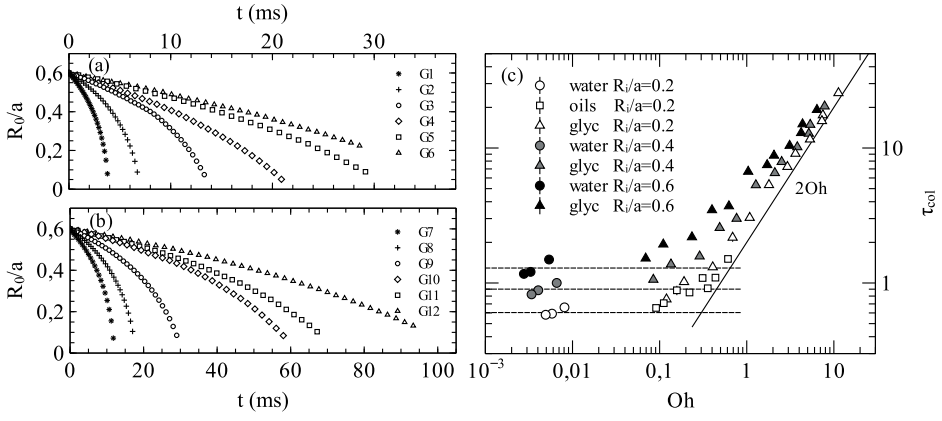

FIG. 2. (a) Temporal evolution of the neck radius, $R_0(t)$, obtained from the experiments with the glycerine-water mixtures G1-G6 and (b) G7-G12 reported in Table I. For clarity, not all the symbols are shown, and the neck radius is made dimensionless with the injector radius, a, so that all the experiments can be represented in a single plot. (c) Dimensionless collapse time extracted from (a) and (b) as a function of Oh for different stages of the collapse process, namely, $R_i/a = 0.2$ (hollow symbols), $R_i/a = 0.4$ (grey symbols), and 0.6 (black symbols). The experiments with silicone oils for $R_i/a = 0.2$ have been taken from Ref. 17. Several experiments with water taken from Ref. 8 have also been added to obtain the inviscid limit $Oh \to 0$. The solid line corresponds to the Stokes limit $Oh \gg 1$, in which $\tau_{col} \to 2\,Oh$, while the dashed line is the inviscid limit given by Eq. (17) for the collapse time, 0.6, 0.9, and 1.29, corresponding to each collapse stage, respectively.

at least five different collapse events, obtaining a very small standard deviation. The corresponding error associated to the averaged values in Figs. 2(b) and 4 was calculated as the maximum between the error associated with the temporal resolution and the standard deviation corresponding to the averaged value. The error bars are plotted in Figs. 2(b) and 4, although they cannot be observed because they are smaller than the symbols that cover them. The resulting dimensionless collapse time, $\tau_{col} = t_{col}/t_\sigma$, where $t_\sigma = (\rho R_i^3/\sigma)^{1/2}$ is the capillary time based on the initial neck radius, is shown in Fig. 2(c) for three different stages of the collapse, namely, $R_i/a = 0.6$, 0.4, and 0.2. To determine the inviscid limit, $Oh \to 0$, several experiments with water are also plotted in Fig. 2(c), taken from Bolaños-Jiménez *et al.*[8] (Nozzles III, VI, and VIII in their Table I, for which $Oh_a = 4.2 \times 10^{-3}$, 2.6×10^{-3}, and 2.1×10^{-3}, respectively). In addition, for the case of $R_i/a = 0.2$, the experiments with silicone oils O1-O8 of Table I in Bolaños-Jiménez *et al.*[17] have also been displayed to contemplate the transition regime, which corresponds to intermediate values of Oh in Fig. 2(c). This figure reveals that the collapse time increases monotonically with both Oh and R_i/a and also that three different regimes can be distinguished: (i) the inviscid limit $Oh \ll 1$, for which τ_{col} tends to a constant that depends only on R_i/a, (ii) the transition regime for $Oh \sim O(1)$, where τ_{col} increases with Oh, and (iii) a linear trend corresponding to the Stokes limit achieved for $Oh \gg 1$, for which $\tau_{col} \to 2Oh$. The value of Oh for which the latter limit is achieved increases with R_i/a.

III. SCALING OF THE COLLAPSE TIME

The present section is devoted to provide a scaling law for the collapse time able to describe the dependence of τ_{col} on Oh and R_i/a shown in the experimental data displayed in Fig. 2(c). To that end, first, the conservation equations are applied to the liquid surrounding the collapsing neck obtaining, as a first approximation, the cylindrical Rayleigh-Plesset (R-P) equation that provides the temporal evolution of the neck radius. Next, by linearizing the R-P equation, a simple analytical expression for the bubble collapse time is obtained.

The shape of the interface near the neck, where the radius takes its minimum value $R_0(t)$, is known to be locally parabolic,[8,12,14,15,25,26] $r_s(z,t) = R_0(t) + r_1(t)\, z^2$, where $r_1(t)$ is the semi-axial curvature evaluated at the neck and z is the axial coordinate, being $z = 0$, which varies with time, the neck position (see Fig. 1(a)). Previous experiments have demonstrated that the local shape around the neck is slender[8,17] since $R_0\, r_1 \ll 1$. Therefore, L/R_0, where $L \propto R_0/(R_0 r_1)^{1/2}$, is the characteristic axial length scale, grows during the collapse process, the local shape evolving towards a cylinder as pinch-off is approached, $R_0\, r_1 \to 0$. Thus, for simplicity, in the following development, the neck is assumed to accomplish the slenderness condition $R_0\, r_1 \ll 1$, and correspondingly, the liquid flow is considered purely radial, $\vec{v} = v(r,t)\, \vec{e}_r$, where $\vec{e}_r$ denotes the unit vector in the radial direction, while $v(r,t)$ is obtained from the liquid continuity equation,

$$v = \frac{\dot{R}_0\, R_0}{r}, \tag{1}$$

where $\dot{R}_0 = dR_0/dt$. The radial momentum equation for the liquid then writes

$$\rho \left[\frac{\ddot{R}_0\, R_0 + \dot{R}_0^2}{r} - \frac{\dot{R}_0^2\, R_0^2}{r^3} \right] = -\frac{\partial p}{\partial r}, \tag{2}$$

where Eq. (1) has been used for the radial velocity, and the viscous term is identically zero due to the fact that the liquid velocity field is irrotational, as shown in Ref. 25. Equation (2) can be integrated in the radial direction inside the liquid surrounding the neck, namely, between $r = R_0(t)$ and a certain point $r = R_c$ placed far away from the neck, $R_c \gg R_0$ to obtain

$$\ln\left(\frac{R_c}{R_0}\right) (R_0\, \ddot{R}_0 + \dot{R}_0^2) - \frac{1}{2}\, \dot{R}_0{}^2 = \frac{p(R_0) - p(R_c)}{\rho}, \tag{3}$$

which is just the cylindrical Rayleigh-Plesset equation, subject to the initial conditions $R_0(t = 0) = R_i$ and $\dot{R}_0(t = 0) = v_i$.

Note that $p(R_0) - p(R_c)$ is the liquid pressure difference driving the collapse, which is established between the interface and the point R_c far away the neck. To obtain this pressure difference, the equilibrium of normal stresses at the interface in the region around the neck must be considered,

$$p_g - p(R_0) + \vec{n} \cdot \bar{\bar{\tau}}' \cdot \vec{n} = \sigma \nabla \cdot \vec{n}, \tag{4}$$

where the viscous stresses in the gas region have been neglected, $\bar{\bar{\tau}}'_g \ll \bar{\bar{\tau}}'$, and the normal viscous stress is given by $\vec{n} \cdot \bar{\bar{\tau}}' \cdot \vec{n} = -2\mu \dot{R}_0 / R_0$. On the other hand, thanks to the slenderness condition, the curvature in Eq. (4) simplifies to $\nabla \cdot \vec{n} = 1/R_0$. Thus, Eq. (4) finally writes

$$p_g - p(R_0) - 2\mu \frac{\dot{R}_0}{R_0} = \frac{\sigma}{R_0}, \tag{5}$$

where the pressure inside the bubble is $p_g = p(R_0) + \sigma/R_0 + 2\mu \dot{R}_0/R_0$. Furthermore, considering p_g uniform and neglecting buoyancy effects, the pressure inside the bubble must be equal to the liquid pressure at $r = R_c$, $p_g = p(R_c)$. Thus, the pressure difference across the liquid field becomes

$$p(R_0) - p(R_c) = -\frac{\sigma}{R_0} - 2\mu \frac{\dot{R}_0}{R_0}. \tag{6}$$

Substituting Eq. (6) into Eq. (3), the Rayleigh-Plesset equation becomes,

$$\ln\left(\frac{R_c}{R_0}\right) \left(R_0 \ddot{R}_0 + \dot{R}_0^2\right) - \frac{1}{2} \dot{R_0}^2 = -\frac{\sigma}{\rho R_0} - 2\mu \frac{\dot{R}_0}{\rho R_0}, \tag{7}$$

with $R_0(t = 0) = R_i$ and $\dot{R}_0(t = 0) = v_i < 0$ as initial conditions. Introducing the dimensionless variables $\eta(\tau) = R_0(t)/R_i$ and $\tau = t/t_\sigma$, with $t_\sigma = (\rho R_i^3/\sigma)^{1/2}$ the capillary time based on the initial neck radius R_i, Eq. (7) can be expressed as

$$\left[\ln\left(\frac{C_1}{\eta}\right) \left(\eta \ddot{\eta} + \dot{\eta}^2\right) - \frac{1}{2} \dot{\eta}^2\right] \eta = -1 - 2\, Oh \dot{\eta}, \tag{8}$$

with the initial conditions $\eta(0) = 1$ and $\dot{\eta}(0) = \dot{\eta}_i = v_i/v_\sigma$, being $v_\sigma = \sqrt{\sigma/(\rho\, R_i)}$ the capillary velocity, and $C_1 = R_c/R_i$.

Equation (8) does not have an analytical solution for $\eta(\tau)$, but it can be solved numerically. In particular, for the inviscid limit, the collapse time, τ_{col}, i.e., the time at which $\eta = 0$, can be calculated by integrating Eq. (8) numerically for $Oh \to 0$. Specifically, the results corresponding to $Oh = 10^{-3}$ are plotted in Fig. 3(a) for $R_i/a = 0.2$ and in Fig. 3(b) for $R_i/a = 0.4$ and $R_i/a = 0.6$, obtaining a collapse time of $\tau_{col} = 0.6\,(R_i/a = 0.2)$, $\tau_{col} = 0.9\,(R_i/a = 0.4)$, and $\tau_{col} = 1.3\,(R_i/a = 0.6)$, in agreement with the experimental values observed in Fig. 2(c) for the three cases for $Oh \ll 1$. The values of the initial velocities considered in Eq. (8), and provided in Table II, have been extracted from the experimental measurements. Moreover, the temporal evolution of the neck radius given by Eq. (8) is able to reproduce the experimental data, as can be observed in Fig. 3(c), where a particular case corresponding to water ($Oh = 3.3 \times 10^{-3}$) is plotted. Note that a good agreement is obtained even though this case corresponds to $R_i/a = 0.6$, and therefore the initial radius is still far from the pinch-off.

For the viscous limit, on the other hand, it is immediate to provide an analytical expression from Eq. (8) for the collapse time valid for $Oh \to \infty$. In this limit, the inertial effects are negligible, and thus, the surface tension effects are balanced with the viscous forces. From Eq. (8), we obtain $1 = 2\, Oh\, \dot{\eta}$, which can be integrated to yield,

$$\int_1^0 d\eta = -\frac{1}{2\, Oh} \int_0^{\tau_{col}} d\tau \;\; \to \tau_{col}(Oh \to \infty) = 2\, Oh. \tag{9}$$

As expected, the collapse time grows linearly with Oh. This viscous limit has been plotted in Fig. 2(c), showing a very good agreement with the experimental data, especially in the case $R_i/a = 0.2$.

The approach adopted in the present work to obtain an analytical expression for the collapse time consists of linearizing Eq. (8). To that end, the dimensionless neck radius is written as

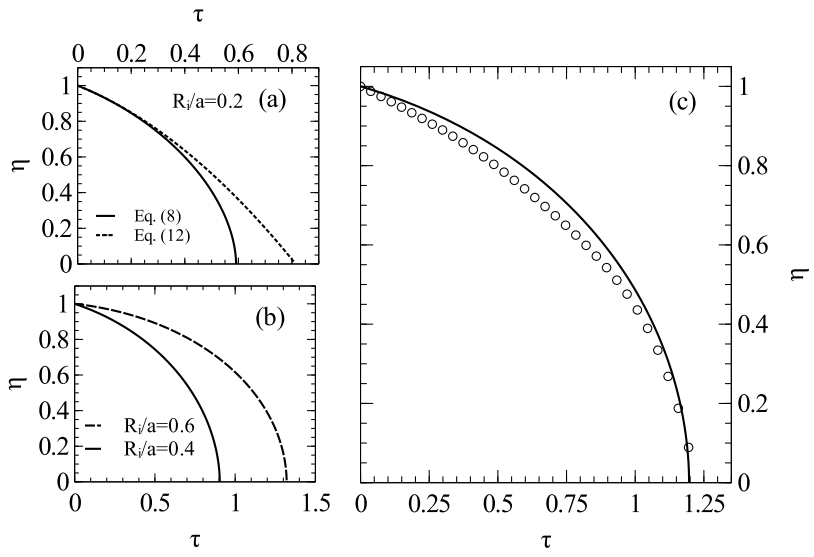

FIG. 3. Temporal evolution of the dimensionless neck radius for the inviscid limit, $Oh \ll 1$. (a) Integration of the Rayleigh-Plesset equation (Eq. (8)) for $Oh = 10^{-3}$, $R_i/a = 0.2$, $\dot{\eta}_i = -0.6$, and $C_1 = 2$ (solid line), together with the result obtained from the linearized version (dotted line), $\eta = 1 - \varepsilon$, with ε given by Eq. (12). (b) Integration of the Rayleigh-Plesset equation (Eq. (8)) for $Oh = 10^{-3}$, $R_i/a = 0.4$ (solid line) with $\dot{\eta}_i = -0.3$ and $C_1 = 5$, and $R_i/a = 0.6$ (dashed line), with $\dot{\eta}_i = -0.1$ and $C_1 = 10$. (c) Integration of Eq. (8) (solid line) for the particular case of $Oh = 0.0033$ and $R_i/a = 0.6$, together with the experimental data (symbols) corresponding to an experiment in water (nozzle VI of Table I in Ref. 8).

$\eta = 1 - \varepsilon(\tau)$, being $0 < \varepsilon(\tau) \ll 1$, and Eq. (8) provides the following linear evolution equation for the perturbed radius $\varepsilon(\tau)$,

$$\ddot{\varepsilon} \ln C + 2\, Oh\, \dot{\varepsilon} = 1 - \left[\frac{1}{2} - \ln C\right] \dot{\epsilon}_i^2, \tag{10}$$

with $\varepsilon(0) = 0$ and $\dot{\varepsilon}(0) = -\dot{\eta}(0) = \dot{\epsilon}_i$ as initial conditions. In Eq. (10), a constant C different from C_1 used in Eq. (8) needs to be introduced since, as it will be shown later, the collapse time is overestimated by the linearized equation if the value of C is retained. Equation (10) can be analytically integrated, giving

$$\varepsilon(\tau) = \frac{1 - (1/2 - \ln C)\dot{\epsilon}_i^2}{2\, Oh}\, \tau - \left(\dot{\epsilon}_i - \frac{1 - (1/2 - \ln C)\dot{\epsilon}_i^2}{2\, Oh}\right) \frac{\ln C}{2\, Oh} \left[\exp\left(-\frac{2\, Oh}{\ln C}\, \tau\right) - 1\right]. \tag{11}$$

Now, if the Taylor expansion of the exponential function is applied to the last term in Eq. (11), one gets

$$\varepsilon(\tau) = \left(\frac{1 - (1/2 - \ln C)\, \dot{\epsilon}_i^2}{2} - \dot{\epsilon}_i\, Oh\right) \frac{\tau^2}{\ln C} + \dot{\epsilon}_i\, \tau. \tag{12}$$

The temporal evolution of the dimensionless neck radius, $\eta = 1 - \varepsilon$, with ε given by Eq. (12), has been plotted in Fig. 3(a) for $Oh = 10^{-3}$ and $R_i/a = 0.2$ with $C = C_1 = 2$. Note that the linearized

TABLE II. Experimental value of the initial neck velocity, $\dot{\eta}_i$, and constants C_1 used in Eq. (8) and C used in Eq. (12) for the three stages of the collapse studied here.

R_i/a	$\dot{\eta}_i$	C_1	C
0.2	−0.6	2	1.2
0.4	−0.3	5	1.5
0.6	−0.1	10	2.3

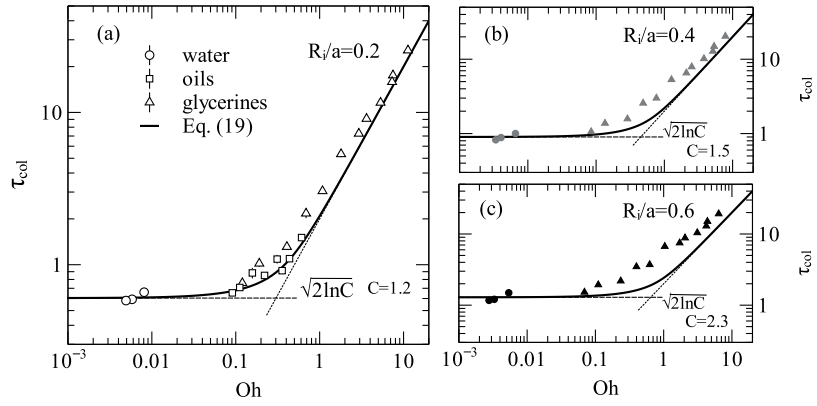

FIG. 4. Dimensionless collapse time as a function of the Ohnesorge number for the three stages: (a) $R_i/a = 0.2$, (b) $R_i/a = 0.4$, and (c) $R_i/a = 0.6$. Symbols correspond to the experiments, while solid lines are the results provided by Eq. (19). The dashed lines represent the inviscid (Eq. (17)) and the viscous (Eq. (9)) limits, respectively.

equation initially follows the result given by the complete Rayleigh-Plesset equation, although it deviates as time evolves, overestimating the collapse time if $C = C_1$ is considered, $\tau_{col} = 0.81 > 0.6$. Therefore, the values of C must be different in linearized Eq. (12) from those used for C_1 in Eq. (8) in order to obtain the correct collapse times.

Let us explore now the limit $Oh \to 0$ in Eq. (12),

$$\varepsilon(\tau)|_{Oh\to 0} = \frac{1 - (1/2 - \ln C)\,\dot{\epsilon}_i^2}{2\,\ln C}\,\tau^2 + \dot{\epsilon}_i\,\tau. \tag{13}$$

In this case, if $\eta = 1 - \varepsilon$ is plotted, the same solution as that obtained with Eq. (12) for $Oh = 10^{-3}$ is obtained in Fig. 3(a). Now, note that Eq. (13) gives the collapse time when $\varepsilon = 1$,

$$\tau_{col}(Oh \to 0) = \left[-\dot{\varepsilon}_i + \sqrt{\dot{\varepsilon}_i^2 + \frac{2[1 - (1/2 - \ln C)\,\dot{\epsilon}_i^2]}{\ln C}}\right] \frac{\ln C}{1 - (1/2 - \ln C)\,\dot{\epsilon}_i^2}. \tag{14}$$

In addition, if $\dot{\varepsilon}_i^2 \ll 2[1 - (1/2 - \ln C)\,\dot{\epsilon}_i^2]/\ln C$, Eq. (14) yields

$$\tau_{col}(Oh \to 0) = \sqrt{\frac{2\,\ln C}{1 - (1/2 - \ln C)\,\dot{\epsilon}_i^2}} - \frac{\dot{\varepsilon}_i\,\ln C}{1 - (1/2 - \ln C)\,\dot{\epsilon}_i^2}, \tag{15}$$

an expression which is valid for $\dot{\varepsilon}_i \ll \sqrt{2/|1 - \ln C|}$. Using the values of C given in Table II, the last condition requires $\dot{\varepsilon}_i \ll 1.6$, 1.8, and 3.5, respectively, a condition accomplished by the experimental measurements. Furthermore, since $|1/2 - \ln C|\,\dot{\epsilon}_i^2 \ll 1$, the following simplified expression for the collapse time can be obtained:

$$\tau_{col}(Oh \to 0) = \sqrt{2\ln C} - \dot{\varepsilon}_i\,\ln C. \tag{16}$$

Given that $\dot{\varepsilon}_i\,\ln C \ll \sqrt{2\ln C}$ for the values of C and $\dot{\varepsilon}_i = -\dot{\eta}_i$ provided in Table II, a collapse time scale independent of the initial velocity and valid in the inviscid limit can be obtained

$$\tau_{col}(Oh \to 0) = \sqrt{2\ln C}. \tag{17}$$

Using the values of C given in Table II, Eq. (17) yields $\tau_{col} = 0.6\,(R_i/a = 0.2)$, $\tau_{col} = 0.9\,(R_i/a = 0.4)$, and $\tau_{col} = 1.29\,(R_i/a = 0.6)$, which are in excellent agreement with the experimental asymptotic values showed in Figs. 2(c) and 4.

Therefore, in the following, a zero initial velocity, $\dot{\varepsilon}_i = 0$, will be assumed in order to obtain a simple scaling for the collapse time valid for any value of Oh. Thus, coming back to Eq. (11),

$$\varepsilon(\tau) = \frac{\tau}{2\,Oh} + \frac{\ln C}{4\,Oh^2}\left[\exp\left(-\frac{2\,Oh}{\ln C}\,\tau\right) - 1\right], \tag{18}$$

which gives the next expression for the collapse time when $\varepsilon = 1$,

$$1 = \frac{\tau_{col}}{2\,Oh} + \frac{\ln C}{4\,Oh^2}\left[\exp\left(-\frac{2\,Oh}{\ln C}\,\tau_{col}\right) - 1\right]. \tag{19}$$

This transcendental Eq. (19) for τ_{col} and Oh provides a scaling law for the collapse time, which has been plotted in Fig. 4 for the three stages, R_i/a, studies here, observing a good agreement with the experimental data for the entire range of Ohnesorge numbers. In particular, note that Eq. (19) reaches both the inviscid (Eq. (17)) and viscous (Eq. (9)) limits. In fact, notice that the agreement between Eq. (19) and the experiments is excellent for the closest stage to the pinch-off ($R_i/a = 0.2$, Fig. 4(a)), while the data deviate from the theory for larger values of the initial radius (Figs. 4(b) and 4(c)) since the neck becomes less slender as R_i/a increases. Consequently, the slenderness condition of the neck assumed in the analysis is better accomplished as the neck approaches to the pinch-off. In addition, it is straightforward to extract both the viscous and inviscid limits from Eq. (19). On the one hand, for $Oh \to \infty$, Eq. (19) gives $1 = \tau_{col}/(2\,Oh)$, providing $\tau_{col}(Oh \to \infty) = 2\,Oh$, which is the same expression as that obtained in Eq. (9) for the collapse time in the viscous limit. On the other hand, for $Oh \to 0$, if the Taylor expansion for the exponential term in Eq. (19) is applied, one gets $1 = \tau_{col}^2/(2\,\ln C)$, and thus $\tau_{col}(Oh \to 0) = \sqrt{2\,\ln C}$, as previously obtained in Eq. (17).

IV. CONCLUSIONS

In this work, an experimental and theoretical analysis of the effect of an arbitrary liquid viscosity on the bubble collapse process has been performed. In the experimental work, the quasi-static collapse of air bubbles inside water-glycerol mixtures with different viscosity, covering a range of 20 cP $\lesssim \mu \lesssim$ 1500 cP, has been investigated. To perform the experiments, two injection needles with different radius, a, have been used, and the temporal evolution of the neck radius, $R_0(t)$, as well as the collapse time, t_{col}, has been obtained analyzing high-speed movies recorded focusing at the length scale of the neck. Additional experiments performed in water, taken from Ref. 8, have been included to examine the inviscid limit, covering thus a range of almost three decades in the Ohnesorge number, $Oh = \mu/\sqrt{\rho\,\sigma\,R_i}$. The dimensionless collapse time, $\tau_{col} = t_{col}/t_\sigma$, with $t_\sigma = (\rho R_i^3/\sigma)^{1/2}$ being the capillary time based on R_i, has been analyzed for three different collapse stages of the necking process, namely, $R_i/a = 0.6$, 0.4, and 0.2. The experimental results revealed that τ_{col} increases with Oh covering three different regimes. In the inviscid limit ($Oh \ll 1$), τ_{col} tends to a constant that increases with R_i/a; in the transition regime ($Oh \sim O(1)$), τ_{col} increases smoothly with Oh; while in the viscous limit ($Oh \gg 1$), τ_{col} increases linearly with Oh as $\tau_{col}(Oh \to \infty) \to 2Oh$.

To describe the bubble pinch-off process, the governing equations have been applied to the liquid field around the collapsing neck, whose shape has been approximated as a time evolving parabola, $r_s(z,t) = R_0(t) + r_1(t)\,z^2$, with r_1 the axial curvature and z the axial coordinate, being $z = 0$ the position of the minimum radius, $R_0(t)$. Since the interface around the neck is slender, that is, $R_0\,r_1 \ll 1$,[8,17] evolving to a cylinder as the time approaches to the pinch-off, $R_0\,r_1 \to 0$, the collapse process has been assumed to be purely radial. Thus, the cylindrical Rayleigh-Plesset can be used to describe the process, provided that $p(R_0) - p(R_c)$, where R_c is a point far from the neck, is the liquid pressure difference leading to the neck collapse. Therefore, the Rayleigh-Plesset equation has been integrated to determine the temporal evolution of the neck radius, as well as the collapse time for three different values of the initial neck radius, i.e., $R_i/a = 0.6$, 0.4, and 0.2. It has been observed that the value of R_c decreases as the initial neck radius, R_i, decreases since the slenderness condition of the neck is better accomplished. Moreover, the collapse time corresponding to the viscous limit, $\tau_{col}(Oh \to \infty) = 2\,Oh$, has been inferred from Eq. (8), showing a very good agreement with the experimental data, in particular for the case closest to the pinch-off event, $R_i/a = 0.2$.

In addition, the Rayleigh-Plesset equation has been linearized to obtain an analytical expression for the collapse time. The linearized equation has been shown to agree with the experimental results for a certain value of the constant C, different from $C_1 = R_c/R_i$, since it deviates from the full Rayleigh-Plesset equation as the pinch-off approaches. Furthermore, assuming a negligible initial neck velocity, an analytical expression for the collapse time given by Eq. (19) and valid for any value of Oh has been obtained. This scaling law has been shown to reproduce the experimental data for the entire range of the Ohnesorge numbers and the different stages of the necking (i.e., different values of R_i/a). Finally, the linearized equation provided close expressions for the inviscid and the viscous limits given by $\tau_{col}(Oh \to 0) = \sqrt{2 \ln C}$ and $\tau_{col}(Oh \to \infty) = 2\,Oh$, respectively, which are in excellent agreement with the experimental data.

ACKNOWLEDGMENTS

This work has been supported by the Spanish MINECO (Subdirección General de Gestión de Ayudas a la Investigación), Junta de Andalucía, and European Funds under Project Nos. DPI2014-59292-C3-1-P, DPI2014-59292-C3-3-P, and P11-TEP7495. Financial support from the University of Jaén, Project No. UJA2013/08/05, is also acknowledged.

[1] E. J. Liu, K. V. Cashman, A. C. Rust, and S. R. Gislason, "The role of bubbles in generating fine ash during hydromagmatic eruptions," Geology **43**(3), 239–242 (2015).
[2] J. F. Davidson and B. O. G. Schuler, "Bubble formation at an orifice in an inviscid liquid," Trans. Inst. Chem. Engrs. **38**, 335–342 (1960).
[3] A. Marmur and E. Rubin, "A theoretical model for bubble formation at an orifice submerged in an inviscid liquid," Chem. Eng. Sci. **31**(6), 453–463 (1976).
[4] M. S. Longuet-Higgins, B. R. Kerman, and K. Lunde, "The release of air bubbles from an underwater nozzle," J. Fluid Mech. **230**, 365–390 (1991).
[5] D. Gerlach, G. Biswas, F. Durst, and V. Kolobaric, "Quasi-static bubble formation on submerged orifices," Int. J. Heat Mass Transfer **48**(2), 425–438 (2005).
[6] S. T. Thoroddsen, T. G. Etoh, and K. Takehara, "Experiments on bubble pinch-off," Phys. Fluids **19**, 042101 (2007).
[7] F. J. Higuera and A. Medina, "Injection and coalescence of bubbles in a quiescent inviscid liquid," Eur. J. Mech. - B-Fluids **25**, 164–171 (2006).
[8] R. Bolaños-Jiménez, A. Sevilla, C. Martínez-Bazán, and J. M. Gordillo, "Axisymmetric bubble collapse in a quiescent liquid pool. Part II. Experimental study," Phys. Fluids **20**, 112104 (2008).
[9] H. N. Oğuz and A. Prosperetti, "Dynamics of bubble growth and detachment from a needle," J. Fluid Mech. **257**, 111–145 (1993).
[10] F. J. Higuera, "Injection and coalescence of bubbles in a very viscous liquid," J. Fluid Mech. **530**, 369–378 (2005).
[11] J. C. Burton, R. Waldrep, and P. Taborek, "Scaling instabilities in bubble pinch-off," Phys. Rev. Lett. **94**, 184502 (2005).
[12] R. Bergmann, D. van der Meer, M. Stijnman, M. Sandtke, A. Prosperetti, and D. Lohse, "Giant bubble pinch-off," Phys. Rev. Lett. **96**, 154505 (2006).
[13] N. C. Keim, P. Moller, W. W. Zhang, and S. R. Nagel, "Breakup of air bubbles in water: Memory and breakdown of cylindrical symmetry," Phys. Rev. Lett. **97**, 144503 (2006).
[14] J. M. Gordillo, A. Sevilla, J. Rodríguez-Rodríguez, and C. Martínez-Bazán, "Axisymmetric bubble pinch-off at high Reynolds numbers," Phys. Rev. Lett. **95**, 194501 (2005).
[15] J. Eggers, M. A. Fontelos, D. M. Leppinen, and J. Snoeijer, "Theory of the collapsing axisymmetric cavity," Phys. Rev. Lett. **98**, 094502 (2007).
[16] J. M. Gordillo and M. A. Fontelos, "Satellites in the inviscid breakup of bubbles," Phys. Rev. Lett. **98**, 144503 (2007).
[17] R. Bolaños-Jiménez, A. Sevilla, C. Martínez-Bazán, D. van der Meer, and J. M. Gordillo, "The effect of liquid viscosity on bubble pinch-off," Phys. Fluids **21**, 072103 (2009).
[18] K. Terasaka and H. Tsuge, "Bubble formation at a single orifice in highly viscous liquids," J. Chem. Eng. Jpn. **23**(2), 160–165 (1990).
[19] J. F. Davidson and B. O. G. Schuler, "Bubble formation at an orifice in a viscous liquid," Chem. Eng. Res. Des. **75**, S105–S115 (1997).
[20] H. Wong, D. Rumschitzki, and C. Maldarelli, "Theory and experiment on the low-Reynolds-number expansion and contraction of a bubble pinned at a submerged tube tip," J. Fluid Mech. **356**, 93–124 (1998).
[21] R. Ramakrishnan, R. Kumar, and N. R. Kuloor, "Studies in bubble formation I. Bubble formation under constant flow conditions," Chem. Eng. Sci. **24**, 731 (1968).
[22] R. Kumar and N. R. Kuloor, "The formation of bubbles and drops," Adv. Chem. Eng. **8**, 255–368 (1970).
[23] K. Terasaka and H. Tsuge, "Bubble formation under constant flow conditions," Chem. Eng. Sci. **48**, 3417–3422 (1993).
[24] M. Ohta, D. Kikuchi, Y. Yoshida, and M. Sussman, "Robust numerical analysis of the dynamic bubble formation process in a viscous liquid," Int. J. Multiphase Flow **37**(9), 1059–1071 (2011).
[25] J. M. Gordillo, "Axisymmetric bubble collapse in a quiescent liquid pool. Part I. Theory and numerical simulations," Phys. Fluids **20**, 112103 (2008).
[26] A. Sevilla, J. M. Gordillo, and C. Martínez-Bazán, "Bubble formation in a coflowing air-water stream," J. Fluid Mech. **530**, 181–195 (2005).